

Propulsion System Performance Resulting From an Integrated Flight/Propulsion Control Design

Duane Mattern
Sverdrup Technology, Inc.
Lewis Research Center Group
Brook Park, Ohio

and

Sanjay Garg
National Aeronautics and Space Administration
Lewis Research Center
Cleveland, Ohio

Prepared for the
AIAA Guidance, Navigation, and Control Conference
sponsored by the American Institute of Aeronautics and Astronautics
Hilton Head, South Carolina, August 10–12, 1992



(NASA-TM-105874)PROPULSION SYSTEM
PERFORMANCE RESULTING FROM AN
INTERGRATED FLIGHT/PROPULSION
CONTROL DESIGN (NASA) 22p

N93-15525

Unclas

G3/07



PROPULSION SYSTEM PERFORMANCE RESULTING FROM AN INTEGRATED FLIGHT/PROPULSION CONTROL DESIGN

Duane Mattern
Sverdrup Technology, Inc.
Lewis Research Center Group
Brook Park, Ohio 44142

Sanjay Garg
National Aeronautics and Space Administration
Lewis Research Center
Cleveland, Ohio 44135

SUMMARY

Propulsion-system-specific results are presented from the application of the integrated methodology for propulsion and airframe control (IMPAC) design approach to integrated flight/propulsion control design for a short-takeoff-and-vertical-landing (STOVL) aircraft in transition flight. The IMPAC method is briefly discussed and the propulsion system specifications for the integrated control design are examined. The structure of a linear engine controller that results from partitioning a linear centralized controller is discussed. The details of a nonlinear propulsion control system are presented, including a scheme to protect the engine operational limits: the fan surge margin and the acceleration/deceleration schedule that limits the fuel flow. Also, a simple but effective multivariable integrator windup protection scheme is investigated. Nonlinear closed-loop simulation results are presented for two typical pilot commands for transition flight: acceleration while maintaining flightpath angle and a change in flightpath angle while maintaining airspeed. The simulation nonlinearities include the airframe/engine coupling, the actuator and sensor dynamics and limits, the protection scheme for the engine operational limits, and the integrator windup protection. Satisfactory performance of the total airframe plus engine system for transition flight, as defined by the specifications, was maintained during the limit operation of the closed-loop engine subsystem.

INTRODUCTION

The concept behind integrated flight and propulsion controls (IFPC) is the management of the interactions between the airframe and the propulsion system to achieve the desired performance of the entire vehicle while reducing the pilot workload. In the past, IFPC had not been necessary because the propulsion system normally generated only a single thrust component and the effects of the airframe on the engine were treated either as disturbances or as performance limits for the aircraft. Recent advances for propulsive systems, such as thrust-vectoring nozzles and the use of multiple nozzles from a single engine core, have increased the flexibility of the control design for aircraft. The Harrier is an example of an aircraft that uses propulsive lift to increase low-speed control effectiveness. Also, vectored thrust is now being used in highly agile aircraft to enhance maneuverability and controllability, for example, for post-stall maneuvers (ref. 1). Vectored thrusts have magnitude and direction and they generate moments because they do not necessarily pass through the aircraft's center of gravity. With propulsive forces and moments being used for more than just forward momentum (pitch control, for example), disturbances to the operation of the engine can influence more than just the forward acceleration of the airframe. Thus, airframe-to-engine coupling, such as (1) inlet distortion due to the angle of attack, the sideslip angle, or hot gas ingestion during hover and (2) bleed flow extraction from the high-pressure compressor for the reaction control system, must be examined more closely during the control design and evaluation.

The literature on IFPC has generally focused on the mission-level aircraft performance specifications and the resulting closed-loop response of the aircraft. In this report the closed-loop performance of the propulsion subsystem that results from the use of the integrated methodology for propulsion and airframe control (IMPAC) design method is examined for the transition flight mode.

The report is organized as follows: A brief review of the IMPAC design methodology outlines the design steps. The vehicle model is then described, including the details of the propulsion system. Next, the propulsion system operational limits and the engine specifications and how they were accounted for in the centralized control design are discussed. The linear engine controller that resulted from the application of the partitioning of the centralized control design is described, and the details of engine control structure are reviewed. The implementation details of the limit protection and the multivariable integrator windup protection are examined. Performance results for the integrated system are shown for two pilot commands typical of the transition flight. Finally, the main results of the paper are summarized.

SYMBOLS

Airframe

ALR_{RCS}	left-roll RCS area, in. ²
ARR_{RCS}	right-roll RCS area, in. ²
ALY_{RCS}	left-yaw RCS area, in. ²
ARY_{RCS}	right-yaw RCS area, in. ²
AP_{RCS}	pitch RCS area, in. ²
h	altitude, ft
p	roll rate, rad/s
q	pitch rate, deg/s
\bar{q}	dynamic pressure, lbf/ft ² (ft/s) ²
RCS	reaction control system
r	yaw rate, deg/s
TLR_{RCS}	left-roll RCS thrust, lbf
TRR_{RCS}	right-roll RCS thrust, lbf
TLY_{RCS}	left-yaw RCS thrust, lbf
TRY_{RCS}	right-yaw RCS thrust, lbf
TP_{RCS}	pitch RCS thrust, lbf
u	axial velocity, ft/s
V	true airspeed, ft/s
\dot{V}	acceleration along flightpath, ft/s ²
v	lateral velocity, ft/s

w	vertical velocity, ft/s
α	angle of attack, deg
β	sideslip angle, deg
$\dot{\beta}$	rate of change of sideslip angle, deg/s
δ_{e_l}	left-elevon deflection, deg
δ_{e_r}	right-elevon deflection, deg
δ_r	rudder deflection, deg
γ	flightpath angle, deg
θ	pitch attitude, deg
ϕ	roll attitude, deg
ψ	heading angle, deg

Engine

A8	aft-nozzle area, in. ²
A78	ventral-nozzle area, in. ²
ANG8	aft-nozzle vectoring angle, deg
ANG79	ventral-nozzle vectoring angle, deg
DP/P	ratio, (P14 - PS14)/P14
ERAM	inlet ram pressure recovery
ETA	ejector butterfly valve angle, deg
FG9	aft-nozzle thrust, lbf
FGE	total ejector thrust, lbf
FGV	ventral-nozzle thrust, lbf
N2	engine fan rotor speed, rpm
N25	engine core rotor speed, rpm
N25R	corrected engine core rotor speed, $N25 \cdot \sqrt{(T_{std}/T25)}$
P1	fan inlet total pressure, psia
P2	recovered inlet pressure, P1·ERAM, psia
P6	tailpipe entrance pressure, psia
P14	fan discharge total pressure in bypass duct, psia

P_{amb}	ambient pressure, psia
PC	combustor
PE3	compressor bleed pressure, psia
PS3	high-pressure-compressor discharge static pressure, psia
PS14	fan discharge static pressure in bypass duct, psia
SM2	fan compressor surge margin
T2	fan inlet temperature, °R
T25	high-pressure-compressor inlet temperature, °R
TE3	compressor bleed temperature, °R
Tm	metal temperature, °R
T_{std}	standard temperature, 518.67 °R
W2R	engine inlet mass flow rate, corrected for temperature
W25	engine core mass flow rate, lbm/s
WB3	RCS bleed mass flow rate, lbm/s
WF36	fuel flow, lbm/hr
Λ	propulsion controller integrator windup protection gain matrix
λ	integrator windup protection scalar gain

General

A_a, B_a, C_a, D_a	matrices defining linear airframe system
$A_{ec}, B_{ec}, C_{ec}, D_{ec}$	matrices defining linear engine controller
a	subscript, airframe
B_{ae}, D_{ae}	engine-to-airframe interface matrices
c	subscript, commanded variables
e	subscript, engine
e	error in tracking command
eL	subscript, engine limited variable
est	subscript, estimated variable
L	subscript, limited variables
x	subscript, horizontal body-axis thrust component
z	subscript, vertical body-axis thrust component
\bar{u}	perturbed input vector
\bar{x}	perturbed state vector
\bar{y}	perturbed output vector

\bar{y}_{ea}	perturbed engine-to-airframe coupling vector
($\dot{\quad}$)	rate of change

IFPC CONTROL DESIGN METHODOLOGY

An IFPC design method called IMPAC that takes into account coupling between the airframe and the propulsion system in the early phases of the control design is currently under development at NASA Lewis Research Center. The details of the IMPAC methodology presented in reference 2 will be briefly reviewed. Figure 1 shows the IMPAC methodology flowchart. As seen from the flow chart, there are six major steps in IMPAC: (1) control model generation; (2) centralized or integrated linear control design; (3) controller partitioning into linear subcontrollers; (4) full-envelope subsystem control design; (5) subsystem nonlinear control design; and (6) full-system evaluation. Steps 1 and 2, the details of the centralized control design, have been presented in references 3 and 4, and step 3, controller partitioning, was presented in reference 5. Step 4 considers controller scheduling and operating mode switching logic. Because this paper only considers the control design around a transition operating point, step 4 is not discussed herein. The discussion of steps 5 and 6, the subsystem nonlinear control design and the integrated system evaluation, will follow after the vehicle model is described.

VEHICLE MODEL

The model discussed here is used to evaluate the control system around the transition design point while considering many of the airframe and propulsion system nonlinearities. Transition is defined as the flight region in which the forces that support the weight of the aircraft shift from predominately aerodynamic lift to propulsive lift. The model of the airframe, a delta-winged E-7D supersonic short-takeoff-and-vertical-landing (STOVL) airframe, is the same linear model that was used in the linear integrated control design discussed in references 3, 4, and 6. The model of the variable-cycle turbofan engine is a nonlinear component-level model (CLM) (ref. 7). As shown in figure 2 the aircraft is equipped with a convergent-divergent, vectorable aft nozzle; a vectorable ventral nozzle; two wing-root-mounted ejectors; a jet reaction control system (RCS); and the aerodynamic control surfaces: left and right elevons and rudder. At the nominal transition design point the propulsion system supports approximately 60 percent of the weight of the aircraft. The ejector and ventral thrusts were adequately distributed to provide the necessary pitch trim for the aircraft. The RCS was not used for trim, so that the nominal compressor bleed flow was zero. The transition flight-mode model to be discussed is representative of a STOVL aircraft during the approach-to-landing task.

A block diagram of the nonlinear airframe plus engine model that was used for the control evaluation is shown in figure 3. The aircraft portion of the model comprised a linear airframe model, a nonlinear model of the airframe actuators, and a nonlinear RCS model. The small-perturbation linear airframe model was generated at an 80-knot, -3° flightpath angle, and 7° pitch attitude flight condition and is of the form

$$\dot{\bar{x}}_a = \mathbf{A}_a \bar{x}_a + \mathbf{B}_a \bar{u}_a + \mathbf{B}_{ae} \bar{y}_{ea}; \quad \bar{y}_a = \mathbf{C}_a \bar{x}_a + \mathbf{D}_a \bar{u}_a + \mathbf{D}_{ae} \bar{y}_{ea} \quad (1)$$

where \bar{u}_a , \bar{y}_a , \bar{y}_{ea} , and \bar{x}_a are the perturbed airframe input, airframe output, engine-to-airframe interface, and state vectors as shown here:

$$\bar{u}_a = [\delta_{e_1}, \delta_{e_r}, \delta_r, \text{TLR}_{\text{RCS}}, \text{TRR}_{\text{RCS}}, \text{TLY}_{\text{RCS}}, \text{TRY}_{\text{RCS}}, \text{TP}_{\text{RCS}}]^T$$

$$\bar{y}_a = [V, \dot{V}, \theta, q, \gamma, \phi, p, \beta, \dot{\beta}, r]^T$$

$$\bar{y}_{ea} = [FG9_x, FG9_z, FGE_x, FGE_z, FGV_x, FGV_z, W2R, \text{ERAM}]^T$$

$$\bar{x}_a = [u, v, w, p, q, r, \phi, \theta, \psi, h]^T$$

The outputs \bar{y}_{ea} and \bar{y}_a are a relevant subset of the available outputs. The airframe actuators, δ_{e_1} , δ_{e_r} , and δ_r , are first order with bandwidths of 20 rads/s, and they include rate and range limits.

The nonlinear RCS model calculates the resultant RCS thrusts corresponding to each RCS nozzle area (ALR_{RCS} , ARR_{RCS} , ALY_{RCS} , ARY_{RCS} , and AP_{RCS}) on the basis of α and \bar{q} , PE3, TE3, and P_{amb} as shown in figure 3. The RCS model also calculates the required RCS bleed mass flow rate, WB3. For the transition flight mode, WB3 is the primary airframe-to-engine coupling.

The propulsion system model that was used in the control evaluation comprised a nonlinear, component-level model (ref. 7) of the engine and nonlinear actuator and sensor models. Figure 4, from reference 8, shows a schematic of the engine components and the station designations. The components are the low-pressure compressor (fan), the high-pressure compressor (HPC), the combustor, the high-pressure turbine (HPT), the low-pressure turbine (LPT), and the exit areas (ventral and aft nozzle and ejectors). The flow for the aft and ventral nozzles and the primary flow for the ejectors are obtained from the mixing plane of the engine where the core and bypass flows mix as shown in figure 4. The secondary air for the ejectors is an entrained airstream that is external to the engine as displayed in figure 2. The two butterfly valve angles that control the primary airflow to the ejectors are commanded identically, so that no differential ejector thrusts are used in this study. The nonlinear engine model state comprised six variables: two rotor speeds (N2 and N25) and four component metal temperatures ($T_{\text{m}_{\text{HPC}}}$, $T_{\text{m}_{\text{PC}}}$, $T_{\text{m}_{\text{HPT}}}$, and $T_{\text{m}_{\text{LPT}}}$). The metal temperatures have very slow dynamics and the rotor speeds dominate the engine dynamic response. The actuator models have delays and range and rate limits for the engine control inputs WF36, A8, ETA, A78, ANG79, and ANG8. Note in figure 3 that the subscript L indicates that these actuator commands have already been subjected to the engine limit protection scheme, which is part of the control to be discussed later. Although the HPC does have stator vanes, the vane angles are on an open-loop schedule, are not adjusted by the dynamic controller, and thus do not appear in figure 3. Note that the WB3 that is calculated by the RCS model is limited as a percentage of the maximum engine core mass flow by limiting the commanded RCS nozzle areas. The sensor models for T25, N25, PS3, and DP/P are linear first-order lags with fixed time constants, except for T25, which has a time constant that is a function of W25. The engine model outputs \bar{y}_e are N2, N25, FG9, FGE, FGV, T25, PS3, SM2, DP/P, W25, TE3, PE3, P6, T2, and P2, and \bar{y}_{ea} is the engine-to-airframe coupling vector as defined in equation (1). SM2 is not a measured output but is provided for evaluation of the engine response near the fan stall line. FG9, FGE, and FGV are used to evaluate the engine control, but the closed-loop system controls the estimated thrusts, which are discussed later. The vector \bar{y}_{ea} acts as an input on the aircraft. The x-z thrust components provide the necessary propulsive forces and moments. W2R and ERAM are used to calculate the inlet drag due to the engine mass flow and the inlet ram pressure recovery.

PROPULSION SYSTEM OPERATIONAL LIMITS

Typical operational limits for a turbofan engine are the fan and core compressor surge margins, the maximum fan and core rotor speeds, the maximum fan turbine inlet temperature (FTIT), the maximum combustor pressure, and the maximum and minimum combustion fuel/air ratios. Of these limited variables, only the combustor pressure, the FTIT, and the rotor speeds are directly measurable. The FTIT measurement is not currently used for control because reliable measurements are lacking. The limits on the unmeasurable variables are reflected back onto the engine control inputs, resulting in input limit schedules that are a function of the measurable engine outputs. Two such limits are the fuel flow acceleration and deceleration (accel/decel) limit and the minimum fan surge margin limit.

The accel/decel schedule is a set of variable bounds on the fuel flow as a function of N_{25} , T_{25} , and P_3 . This limit schedule is determined a priori by using an open-loop nonlinear simulation of the engine. The schedule imposes a rate limit on core rotor speed as a function of the minimum and maximum fuel/air ratios (lean and rich blowout), the maximum turbine temperature, and the compressor surge margin, as shown in figure 5, from reference 9. The accel/decel limit is reflected back on the engine control input by imposing a limit schedule on the fuel/air ratio. The fuel/air ratio is a function of the WF_{36}/P_3 ratio because the HPC discharge pressure is indicative of the combustor air mass flow rate. The accel/decel schedule is implemented as minimum and maximum bounds on the WF_{36}/P_3 ratio as a function of the corrected core rotor speed, N_{25R} . An example turbofan engine limit schedule from reference 10 shows a normalized WF_{36}/P_3 ratio as a function of N_{25R} in figure 6. In figure 6 the α_1 "droop lines" are lines of constant engine thrust for fixed inlet conditions. The rotor speed schedule determines the "steady state line." A typical engine acceleration from α_1 to α_2 is shown in figure 6. Note how the normalized WF_{36}/P_3 ratio increases at nearly constant rotor speed because of the rotor speed lag. Once the accel limit is reached, WF_{36}/P_3 follows the accel limit until the desired thrust setting is obtained. Finally, WF_{36}/P_3 settles down until the steady-state line is reached. Note that when WF_{36}/P_3 is determined by the accel limit, the fuel flow is determined by the engine outputs, P_3 and N_{25R} . The feedback of these variables links the rate of change of fuel flow (\dot{WF}_{36}) to the rate of change of the core rotor speed (N_{25}) whenever the fuel flow limit is encountered. Thus, the accel/decel limit defines the large-perturbation performance of the engine (assuming no special thrust wasting or off-design schedule engine operating mode). Other limits, such as the maximum fan speed and the minimum combustor pressure, also affect fuel flow, but they were not found to be critical during the transition flight mode and are not considered herein.

The minimum fan surge margin is another critical limit in turbofan engines. Figure 7, from reference 11, shows how the fan surge margin decreases during engine deceleration for a turbofan engine with an appropriately scheduled nozzle area. During a gross thrust decrease on a turbofan engine the surge margin decreases quickly as the fan pressure ratio increases. With the surge margin limited, the much slower fan rotor speed follows along the surge limit line until the desired operating point is reached. The surge margin cannot be directly measured, but it can be correlated with a function of the "delta P over P" pressure ratio (DP/P) as discussed briefly in references 11 and 12. Therefore, it is possible to limit the fan surge margin by limiting DP/P . Imposing a limit schedule on the minimum value of DP/P imposes a varying minimum value on the total engine flow exit area. If the total exit area decreases too quickly, backpressure builds up across the fan and DP/P drops. The limit protection scheme will then increase the total exit area to keep DP/P , and thus the fan surge margin, above the minimum value. In a multi-nozzle engine all the nozzles contribute to the total area, and they all have an effect on the fan surge margin through the bypass duct as can be seen in figure 4. The distribution of the limit protection total area increase over the available nozzles is part of the integrated control design.

The linear integrated control design has been discussed in detail in reference 3, but the propulsion specifications in the integrated control design are discussed here. Before setting up the "design plant" (i.e., the linear model used in the H_∞ design, which in reference 3 included scalings, frequency weights, and internal noise models to build in robustness to specific uncertainties), an open-loop analysis was performed on the system models. In order to gain an understanding of the limit operation of the propulsion system, an open-loop analysis was performed on the engine model with the limit protection scheme in place, as shown in figure 8. From this open-loop analysis it was determined how close the nominal operating point was to the limits, to what extent the actuators could be used before limits were imposed, and what gross effect the limits have on the thrust response (i.e., the region of validity of the small-perturbation linear engine model was determined relative to the operational limits). This information was used in selecting the weights that were used in the linear integrated design. For example, at the design point the accel schedule was reached when the fuel flow was stepped by approximately 600 lbm/hr. The maximum fuel flow available is in the tens of thousands. Using 1000 lbm/hr for scaling the fuel flow in the integrated design instead of the maximum value possible reduced the probability that the fuel flow limit schedule would be encountered. Similarly, when a first-order model was selected to represent the fuel flow actuator in the linear design plant, the bandwidth of this model was based on the phase response of the non-linear actuator because fuel flow has a significant phase lag due to the fuel transportation delay. This open-loop analysis of the propulsion model with the limit protection scheme in place documented the small- and large-perturbation thrust response of the engine. The engine still encounters limits whenever large thrust changes are requested and thus limit protection is still required, but using this information in the integrated control design develops a system that only encounters the engine limits for large-perturbation pilot inputs. Examples of typical, large-perturbation pilot inputs that drive the propulsion system into the limits are discussed shortly.

DESCRIPTION OF ENGINE CONTROLLER

Application of step 2 in the IMPAC methodology (linear integrated control design) resulted in a linear, time-independent, state-space controller at the design point (ref. 4). Applying step 3 (controller partitioning) resulted in the partitioning of the linear centralized controller into lateral and longitudinal controllers. The longitudinal controller was specified to have a hierarchical structure composed of a longitudinal airframe controller and an engine controller. The longitudinal airframe controller calculates three thrust commands that are tracked by the propulsion control. The partitioned propulsion control is completely separate from the airframe controller. This is important so that engine manufacturers can benchtest the propulsion control system independently of the airframe and airframe controller.

The details of the overall engine controller that is built around the partitioned, linear controller are shown in figure 9. The linear partitioned engine controller is of the form

$$\dot{\bar{x}}_{ec} = \mathbf{A}_{ec}\bar{x}_{ec} + \mathbf{B}_{ec}\bar{y}_{ec}; \quad \bar{u}_{ec} = \mathbf{C}_{ec}\bar{x}_{ec} + \mathbf{D}_{ec}\bar{y}_{ec} \quad (2)$$

where \bar{y}_{ec} , \bar{u}_{ec} , and \bar{x}_{ec} are the perturbed engine controller input, output, and state vectors; the first two are described here:

$$\bar{y}_{ec} = [e_{N2}, e_{FG9}, e_{FGE}, e_{FGV}, N2, WB3_{est}]^T$$

$$\bar{u}_{ec} = [WF36_c, A8_c, ETA_c, A78_c]^T$$

The longitudinal airframe controller commands thrusts from the three nozzles, $FG9_c$, FGE_c , and FGV_c . The engine controller uses these commands to determine the fan speed command that is based on the fan speed schedule. The controller then regulates $N2$ and the three thrusts. Thrust is not measured directly, but a nonlinear estimator is used to estimate the three thrusts. As shown in figure 9 the inputs to the thrust estimator are the sensed values for the actuators $WF36$, $A8$, ETA , and $A78$, the engine outputs $P6$, $N2$, DP/P , $T2$, and $P2$, the estimated RCS bleed flow $WB3_{est}$, and P_{amb} . We are using the nonlinear RCS model to generate $WB3_{est}$. The error between the estimated thrust and the thrust computed by the engine model is less than 3 percent of the engine model thrust for both steady-state and dynamic values. This error can be large in terms of perturbation quantities for a linear system. Because the engine controller tracks the commanded thrusts with estimated thrusts, it is important to ensure that thrust estimation errors do not lead to degradation in the integrated system performance.

The partitioned linear controller yielded good small perturbation performance, but even with the scaling in the design plant to help distribute the control authority in order to avoid the engine limits, it was known early in the design that the engine will encounter limit operation in order to meet the extremes of the integrated system performance. The limit protection scheme and the accompanying integrator windup protection scheme are discussed in the next section.

IMPLEMENTATION OF PROPULSION CONTROL LIMIT OPERATION

The two primary engine limits that are encountered in the transition mode are the accel schedule for the fuel flow and the fan surge margin. The accel schedule and fan surge margin limit protection schemes from reference 13 were implemented as engine limit schedules, shown as a block in figure 9. The accel/decel schedule is similar to the scheme for the F100 engine that was previously described. The scheme for protecting the fan surge margin is implemented as previously discussed, by limiting the minimum value for DP/P . If the DP/P limit is reached, all of the nozzle areas are opened by a percentage of their contribution to the total nozzle area. Thus, the fan surge margin limit is shared over all three nozzles (aft, ventral, and ejectors), and all three thrusts are affected when the fan surge margin is reached. Alternative fan surge margin protection schemes that take advantage of redundancies in the pitch control of the airframe are possible but have not yet been investigated.

When the outputs of a controller are limited, the controller integrator must be constrained to prevent integrator windup. Windup is defined as an open-loop, unbounded increase in the magnitude of a controller integrator that does not manifest itself as an increase in the magnitude of the value of the actuator that is seen by the airframe. There is a disconnect between the value calculated by the control and the actuator-commanded value. In the control literature, little attention has been given to developing integrator windup protection schemes for general multivariable controllers. However, reference 13 does a good job of pulling together many of the existing antiwindup schemes. The following discussion is based on the general antiwindup and bumpless transfer (AWBT) scheme discussed in reference 13. Figure 10 is a detailed block diagram of the implementation of the "tracking mode" version of the AWBT scheme. The AWBT action is based on modifying the controller state variable by using the difference between the limited and the commanded actuator values, $e_u = u_{eL} - u_{ec}$, such that the modified controller outputs track the limited actuator values. The integrator windup protection gain matrix Λ , is defined as $\Lambda = \lambda C_{ec}^*$, where C_{ec}^* is the pseudoinverse of C_{ec} . The modified controller then has the form

$$\begin{aligned}\dot{x}_{ec} &= A_{ec}x_{ec} + B_{ec}y_{ec} + \Lambda e_u \\ u_{ec} &= C_{ec}x_{ec} + D_{ec}y_{ec}\end{aligned}\tag{3}$$

By using the definition of e_u , the modified controller state equation can be written as

$$\dot{x}_{ec} = (\mathbf{A}_{ec} - \lambda \mathbf{C}_{ec}^* \mathbf{N} \mathbf{C}_{ec}) x_{ec} + (\mathbf{B}_{ec} - \lambda \mathbf{C}_{ec}^* \mathbf{N} \mathbf{D}_{ec}) y_{ec} + \mathbf{A} u_{eL} \quad (4)$$

where \mathbf{N} is a diagonal matrix of ones and zeros with the ones corresponding to a limited actuator and the zeros corresponding to the unlimited actuators. For this example, a one in the (1,1) element of the \mathbf{N} matrix would indicate that the fuel flow was limited. Similarly, ones in the (2,2), (3,3), and (4,4) elements would indicate that the fan surge margin limit was encountered. Ideally, the product $\mathbf{C}_{ec}^* \mathbf{N} \mathbf{C}_{ec}$ results in a diagonal matrix, and the scalar value λ is used to push the diagonal elements of the modified controller \mathbf{A} matrix farther into the left half-plane. This AWBT action results in a mode switch, so that the controller now regulates the actuator command at the limited actuator value while maintaining the original control objectives of tracking the specified commands. Because \mathbf{C}_{ec} is not an invertible square matrix, it is not possible to speed up all of the engine controller poles. No detailed analyses on the robustness of this AWBT scheme have yet been performed.

To demonstrate the effect of integrator windup protection (IWP), figure 11 compares the response of the closed-loop propulsion system with and without the integrator windup protection for an large $FG9_c$ step command. This $FG9_c$ request encounters a hard fuel flow limit because it requests more than the maximum thrust that the engine can deliver. Figure 11(a) shows the steady-state error that develops in $FG9$ when the hard limit is encountered. Figure 11(b) shows the corresponding limited fuel flows ($WF36_L$) for the two cases and the $WF36_c$ that is commanded by the linear controller for the case without integrator windup protection (without IWP). Note how $WF36_c$ grows unbounded whereas the actuator response is limited. When $FG9_c$ returns to the initial value, the system without IWP takes longer to come off the limit, as shown in figure 11(b), owing to the time taken by the controller integrator to unwind. This delays the $FG9$ response and also increases the coupling to the other nozzles as shown by the FGV response in figure 11(c). In summary, the AWTB scheme offers good limit tracking while keeping the regulated variables near the commanded values for a variety of inputs.

PERFORMANCE EVALUATION RESULTS FOR PILOT INPUTS

Several representative pilot inputs were used to evaluate the performance of the integrated system in the presence of the engine operation limits. In the transition flight mode, typical pilot control tasks are acceleration or deceleration to a desired airspeed while maintaining flightpath angle or change to a desired flightpath angle while maintaining airspeed. The response of the closed-loop system consisting of the airframe plus engine model as shown in figure 3, the engine controller as shown in figure 10, and the airframe flight controller as described in reference 4 is discussed in the following. An emphasis is placed on comparing the system responses with and without active engine limit protection.

Figure 12 shows the vehicle response to a pilot-commanded deceleration of 0.2 g's to decrease the forward velocity by 20 ft/s. Note that velocity responses for the limited (limit protection active) and unlimited (limit protection disabled) systems are very similar as shown in figure 12(a). For the case with limit protection active, $WF36$ rides the accel schedule for the interval from 3 s to 8 s as shown in figure 12(b). For the case with limit protection disabled, $WF36$ actually exceeds the corresponding accel schedule for an interval from 3 s to 5 s. Note that the accel schedule is different for the limits-active and limits-disabled cases because it is based on the engine outputs, which are different for the two cases. Figure 12(c) shows that the case with limit protection active does have slightly more coupling in the flightpath angle, which is due to the difference in the FGV responses shown in figure 12(d). In both cases the

fan surge margin limit is not reached. The response is interesting in that the deceleration of the airframe has an end result of "accelerating" the engine. Note that the fuel flow is initially reduced to reduce the aft nozzle thrust but is then increased to increase the ejector and ventral nozzle thrusts in order to compensate for the lost aerodynamic lift.

Figure 13 shows the airframe and engine responses to a 4° commanded increase in flightpath angle. This command is essentially a vertical lift command and requires a large increase in thrust. Figures 13(a) to (c) compare the airframe response for a controller with and without active limit protection. The flightpath and velocity responses are very close in the two cases. There is a slight increase in the pitch coupling with the limit protection active, but the response in both cases shows good decoupling from flightpath command. Figure 13(d) shows the engine fuel flow responses for the same command. The system with limit protection rides the accel schedule for the interval from 0.2 s to 2.2 s. The encounter with the accel schedule also slows the fan speed response relative to the case with no limit protection, but the steady-state fan speed schedule is maintained. The nominal operating point is such that on this maneuver the fan surge margin limit is only touched briefly around 2 s. The unlimited case does exceed the fan surge margin limit. Figure 14 compares the airframe-commanded, estimated, and actual (engine CLM output) ejector thrust responses to the flightpath command for the system with limit protection active. In this figure the steady-state bias between the actual and estimated or commanded thrusts has been removed so that at time zero all the perturbed thrusts are zero. Note that while there is some mismatch between the actual and estimated thrust, the airframe responses shown in figure 13 are not adversely affected.

SUMMARY OF RESULTS

This paper describes the propulsion-system-specific results of a closed-loop integrated flight and propulsion control system that resulted from using the integrated methodology for propulsion and airframe control design method. A brief review of the methodology was given along with a discussion of how the propulsion system specifications appear in the integrated design. The operational limits for turbofan engines were discussed, and a limit protection scheme and a multivariable, integrator windup protection scheme were demonstrated in simulation. Simulated, closed-loop, time history responses demonstrated that the engine limit protection can be wrapped around the partitioned linear engine controller without adversely affecting the integrated system response to appropriate pilot-commanded inputs for the transition flying task.

REFERENCES

1. Gal-Or, B.: *Vectored Propulsion, Supermaneuverability and Robot Aircraft*. Springer-Verlag, New York, 1990.
2. Garg, S., et al.: *IMPAC—An Integrated Methodology for Propulsion and Airframe Control*. NASA TM-103805, 1991.
3. Garg, S.; and Ouzts, P.J.: *Integrated Flight/Propulsion Control Design for a STOVL Aircraft Using H-Infinity Control Design Techniques*. NASA TM-104340, 1991.
4. Garg, S.; and Mattern, D.L.: *Application of an Integrated Flight/Propulsion Control Design Methodology to a STOVL Aircraft*. AIAA Paper 91-2792, 1991.

5. Garg, S.: Controller Partitioning for Integrated Flight/Propulsion Control Implementation. Presented at the 1992 American Control Conference, Chicago, IL, June 1992.
6. Akhter, M.M., et al.: Simulation Development for U.S./Canada ASTOVL Controls Technology Program. Proceedings of the Twentieth Annual Pittsburgh Conference on Modeling and Simulation, W.C. Vogt and M.H. Mickle, eds., Instrument Society of America, Research Triangle Park, NC, 1989.
7. Drummond, C.K.; and Ouzts, P.J.: Real-Time Simulation of a STOVL Turbofan Engine. NASA TM-102409, 1989.
8. Adibhatla, S., et al.: GE Aircraft Engines STOVL Multivariable Propulsion Control. General Electric, Cincinnati, OH, 1989.
9. Sobey, A.J.; and Suggs, A.M.: Control of Aircraft and Missile Powerplants. An Introduction to the Analysis and Design of Engine Control Systems. John Wiley & Sons, Inc., New York, 1963, p. 185.
10. Arpasi, D.J.; Cwynar, D.S.; and Wallhagen, R.E.: Sea-Level Evaluation of Digitally Implemented Turbojet Engine Control Functions. NASA TN D-6936, 1972.
11. F100 Multivariable Control Synthesis Program, Volume 1—Development of F100 Control System. Report AFAPL-TR-77-35-VOL-1. Systems Control, Inc., Palo Alto, CA, 1977.
12. Beattie, E.C.: Control Mode Studies for Advanced Variable-Geometry Turbine Engines. Report AFAPL-TR-75-7, Air Force Aero-Propulsion Laboratory, Pratt & Whitney Aircraft, East Hartford, CT, 1974, pp. 13-15.
13. Campo, P.J.; Morari, M.; and Nett, C.N.: Multivariable Anti-Windup and Bumpless Transfer: A General Theory. Proceedings of the 1989 American Control Conference, Vol. 2, AIAA, New York, 1989, pp. 1706-1711.

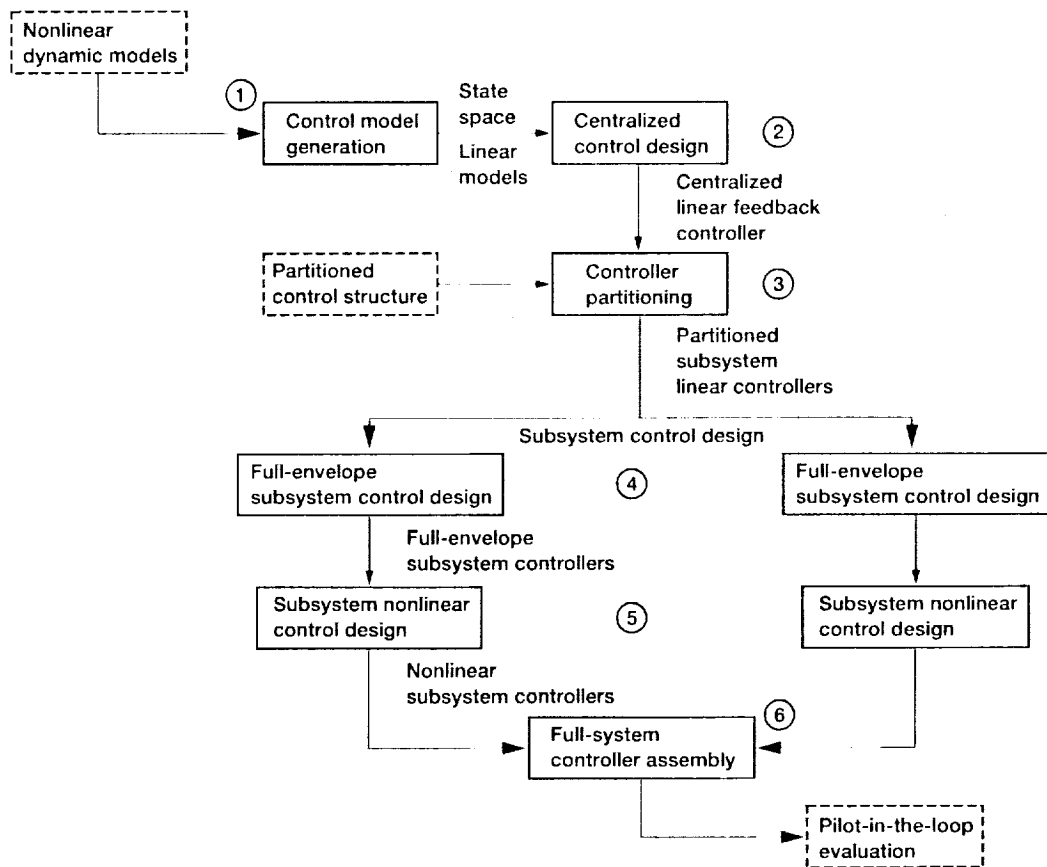


Figure 1.—IMPAC methodology flowchart.

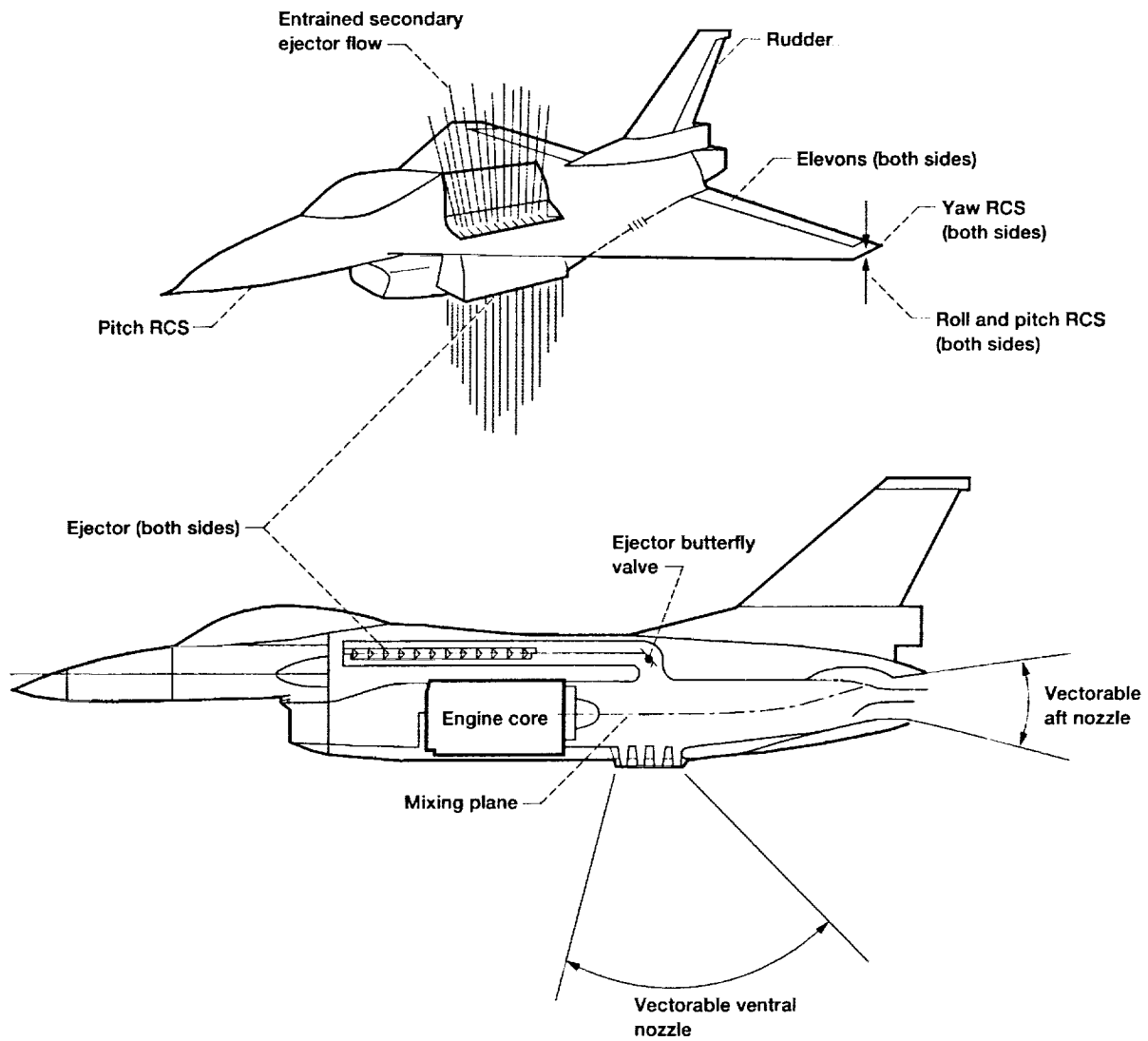


Figure 2.—STOVL aircraft configured with ejectors.

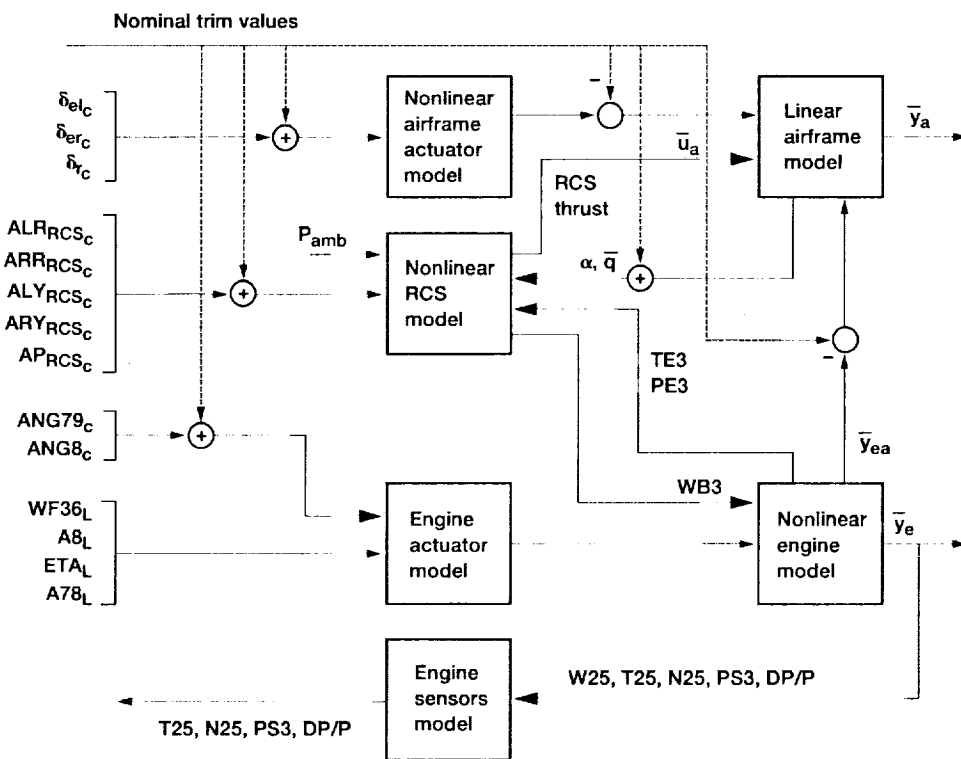


Figure 3.—Overall block diagram of nonlinear model.

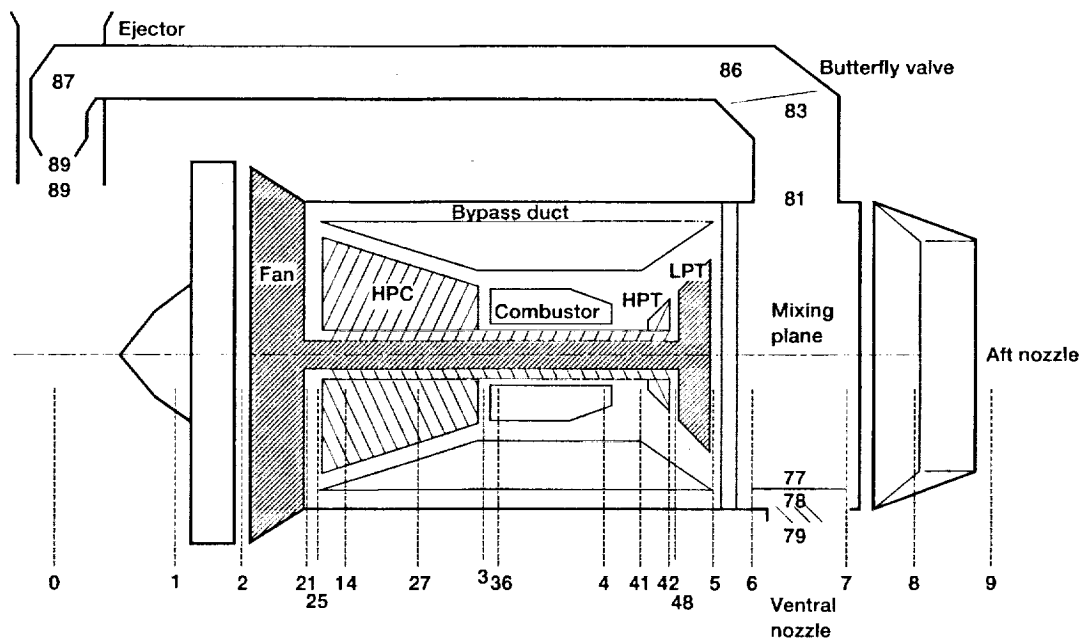


Figure 4.—Schematic of turbofan engine showing station designations. From reference 8.

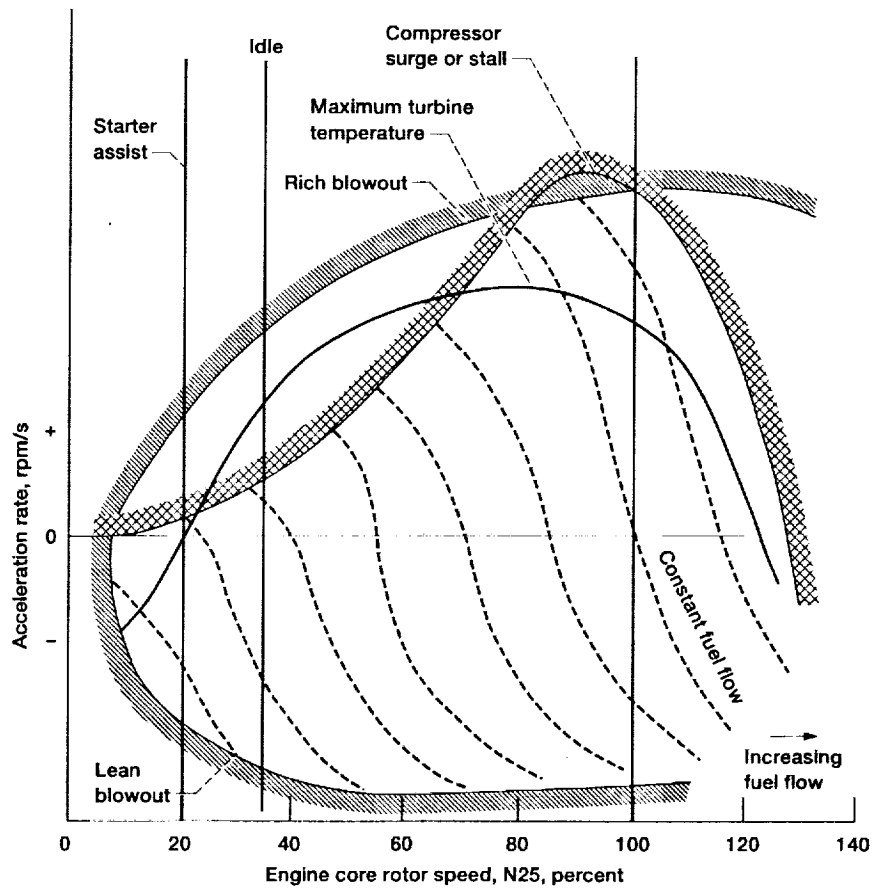


Figure 5.—Typical turbojet acceleration limits. From reference 9.

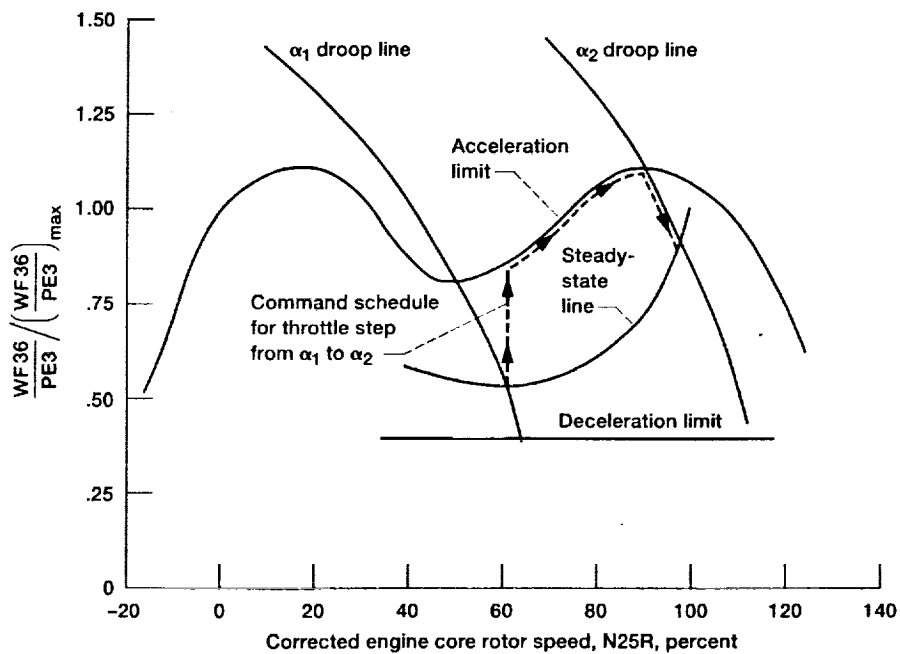


Figure 6.—Typical engine fuel control operating map showing acceleration and deceleration limits. From reference 10.

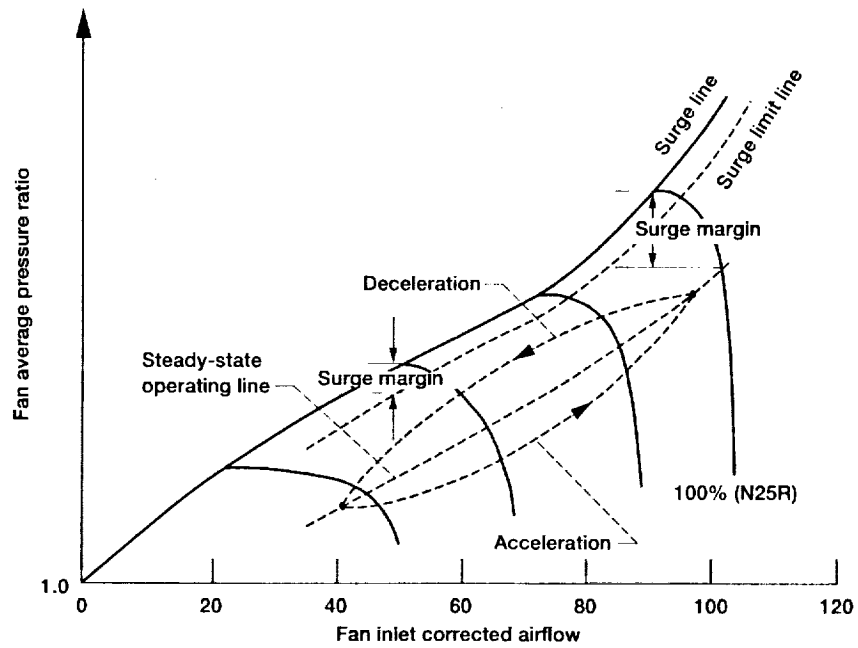


Figure 7.—Fan surge margin change during transient (F100 engine with scheduled nozzle area). From reference 11.

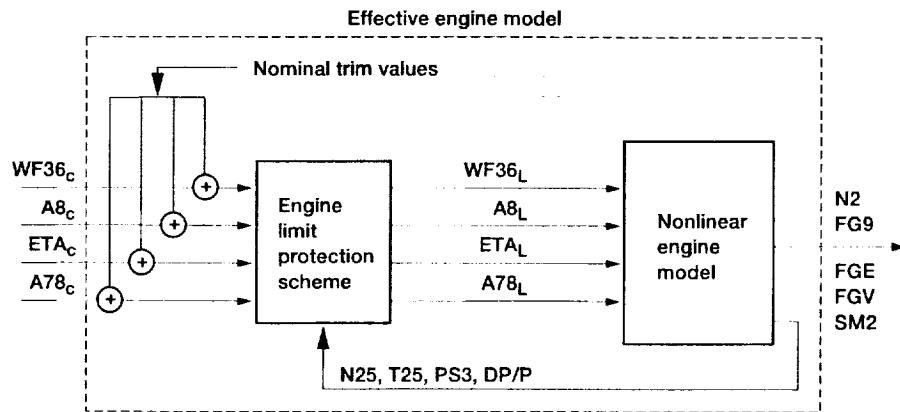


Figure 8.—Open-loop analysis of propulsion system with limits.

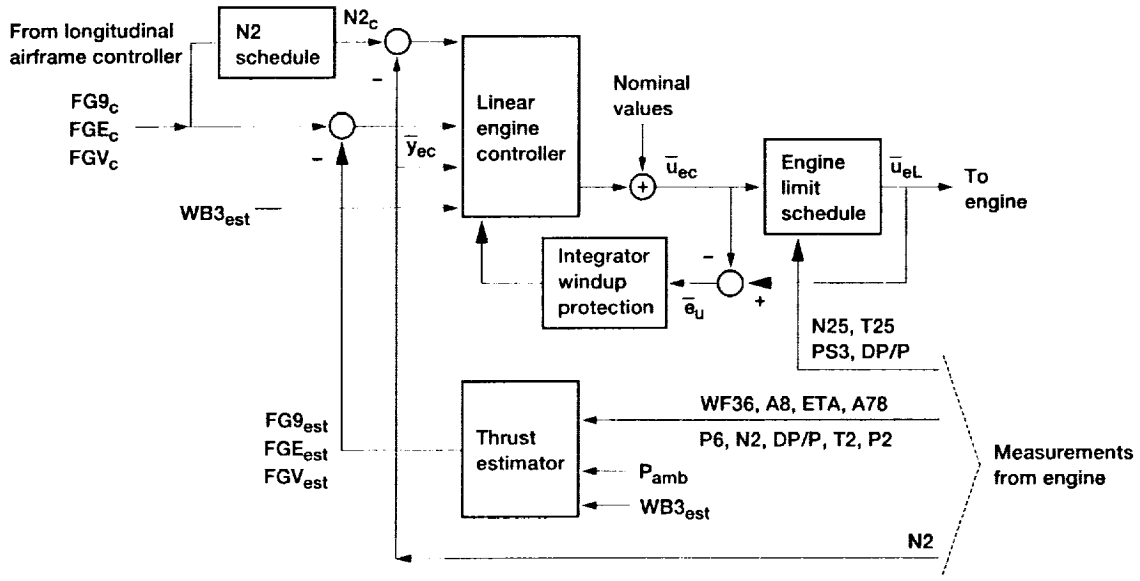


Figure 9.—Detailed block diagram of engine controller.

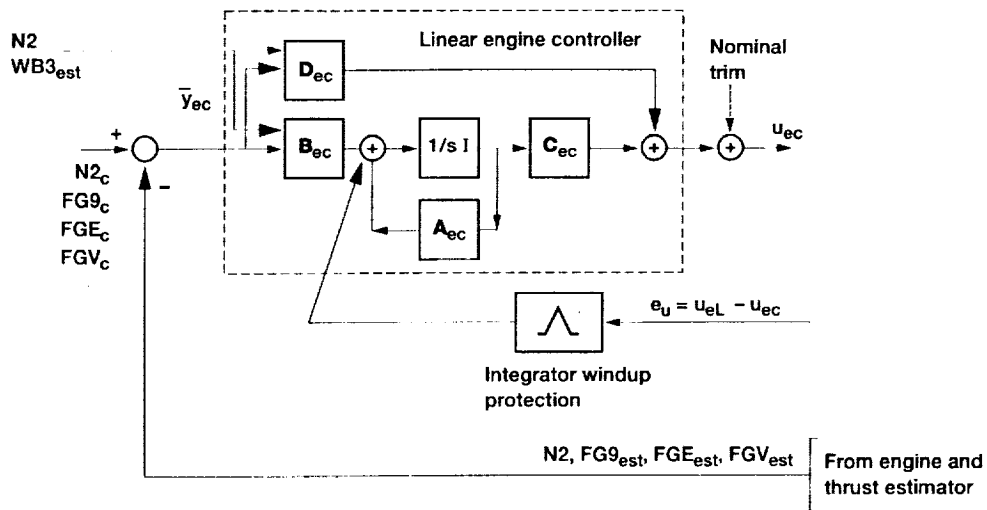


Figure 10.—Detailed block diagram of limit and integrator windup protection.

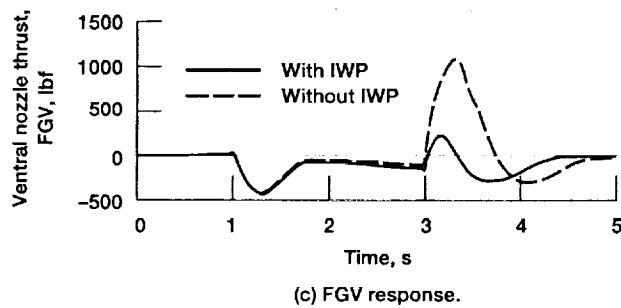
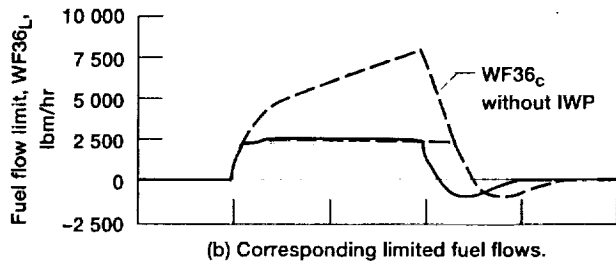
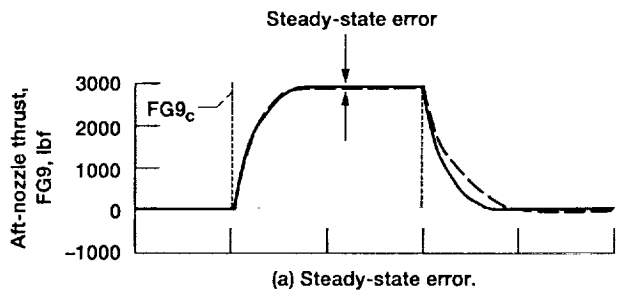


Figure 11.—Effects of integrator windup protection for a 3000-lbf step thrust command.

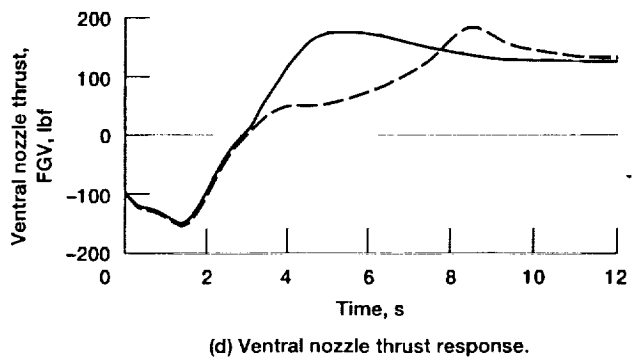
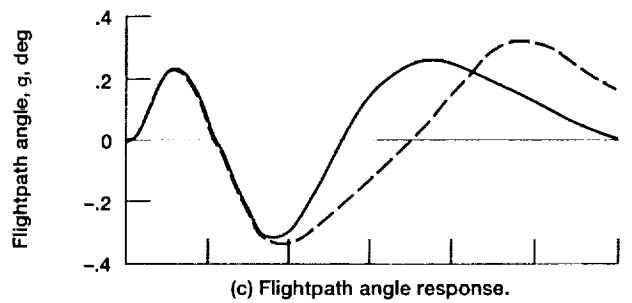
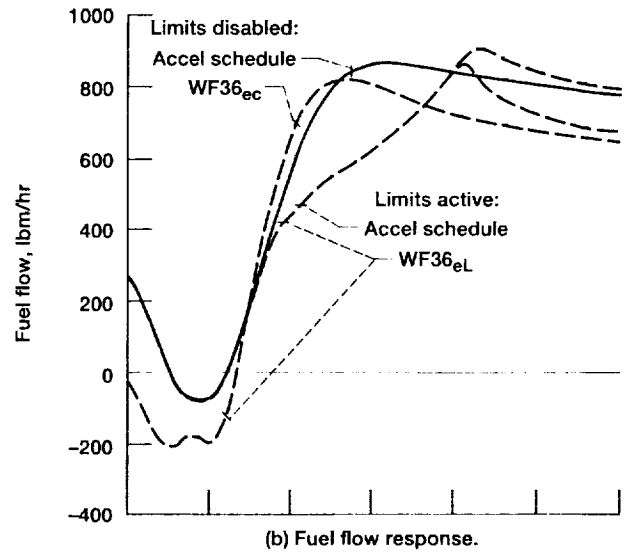
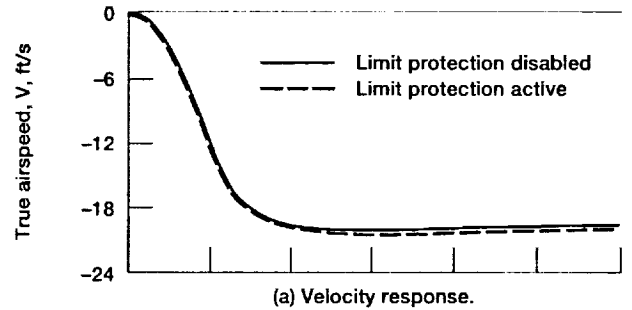
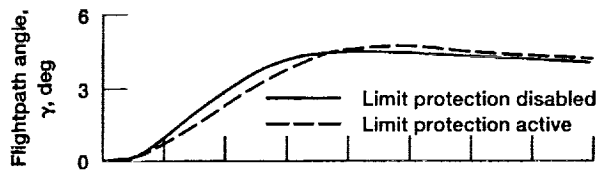
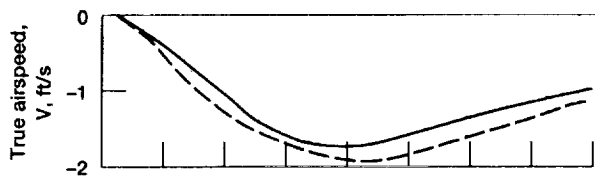


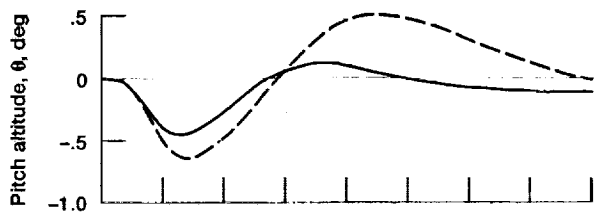
Figure 12.—Comparison of response to deceleration command for systems with and without active limit protection.



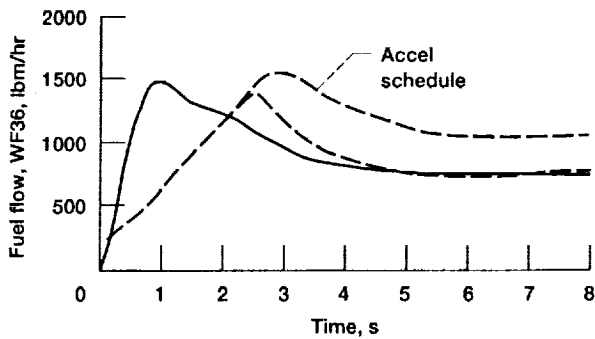
(a) Flight path angle response.



(b) True airspeed response.



(c) Pitch altitude response.



(d) Fuel flow response.

Figure 13.—Comparison of responses to $\gamma_c = 4^\circ$ step command for systems with and without active limit protection.

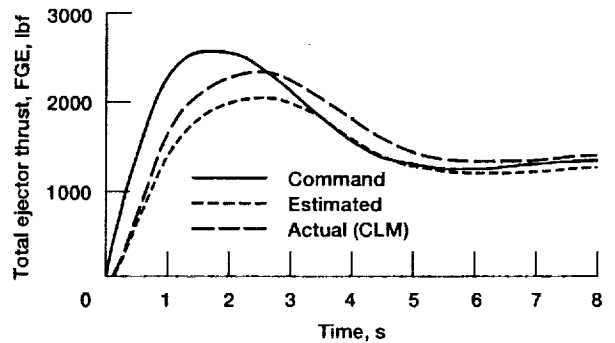


Figure 14.—Comparison of commanded, estimated, and component-level model thrust responses to $g_c = 4^\circ$ step command.

REPORT DOCUMENTATION PAGE

Form Approved
OMB No. 0704-0188

Public reporting burden for this collection of information is estimated to average 1 hour per response, including the time for reviewing instructions, searching existing data sources, gathering and maintaining the data needed, and completing and reviewing the collection of information. Send comments regarding this burden estimate or any other aspect of this collection of information, including suggestions for reducing this burden, to Washington Headquarters Services, Directorate for Information Operations and Reports, 1215 Jefferson Davis Highway, Suite 1204, Arlington, VA 22202-4302, and to the Office of Management and Budget, Paperwork Reduction Project (0704-0188), Washington, DC 20503.

1. AGENCY USE ONLY (Leave blank)		2. REPORT DATE October 1992	3. REPORT TYPE AND DATES COVERED Technical Memorandum	
4. TITLE AND SUBTITLE Propulsion System Performance Resulting From an Integrated Flight/Propulsion Control Design			5. FUNDING NUMBERS WU-505-62-50	
6. AUTHOR(S) Duane Mattern and Sanjay Garg				
7. PERFORMING ORGANIZATION NAME(S) AND ADDRESS(ES) National Aeronautics and Space Administration Lewis Research Center Cleveland, Ohio 44135-3191			8. PERFORMING ORGANIZATION REPORT NUMBER E-7339	
9. SPONSORING/MONITORING AGENCY NAMES(S) AND ADDRESS(ES) National Aeronautics and Space Administration Washington, D.C. 20546-0001			10. SPONSORING/MONITORING AGENCY REPORT NUMBER NASA TM-105874	
11. SUPPLEMENTARY NOTES Prepared for the AIAA Guidance, Navigation, and Control Conference sponsored by the American Institute of Aeronautics and Astronautics, Hilton Head, South Carolina, August 10 - 12, 1992. Duane Mattern, Sverdrup Technology, Inc., Lewis Research Center Group, 2001 Aerospace Parkway, Brook Park, Ohio 44142; and Sanjay Garg, Lewis Research Center, Cleveland, Ohio. Responsible person, Sanjay Garg, (216) 433-8186.				
12a. DISTRIBUTION/AVAILABILITY STATEMENT Unclassified - Unlimited Subject Categories 7 and 8			12b. DISTRIBUTION CODE	
13. ABSTRACT (Maximum 200 words) Propulsion-system-specific results are presented from the application of the integrated methodology for propulsion and airframe control (IMPAC) design approach to integrated flight/propulsion control design for a short-takeoff-and-vertical-landing (STOVL) aircraft in transition flight. The IMPAC method is briefly discussed and the propulsion system specifications for the integrated control design are examined. The structure of a linear engine controller that results from partitioning a linear centralized controller is discussed. The details of a nonlinear propulsion control system are presented, including a scheme to protect the engine operational limits: the fan surge margin and the acceleration/deceleration schedule that limits the fuel flow. Also, a simple but effective multivariable integrator windup protection scheme is investigated. Nonlinear closed-loop simulation results are presented for two typical pilot commands for transition flight: acceleration while maintaining flightpath angle and a change in flightpath angle while maintaining airspeed. The simulation nonlinearities include the airframe/engine coupling, the actuator and sensor dynamics and limits, the protection scheme for the engine operational limits, and the integrator windup protection. Satisfactory performance of the total airframe plus engine system for transition flight, as defined by the specifications, was maintained during the limit operation of the closed-loop engine subsystem.				
14. SUBJECT TERMS Aircraft control; Propulsion; Propulsion control; Integration			15. NUMBER OF PAGES 22	
			16. PRICE CODE A03	
17. SECURITY CLASSIFICATION OF REPORT Unclassified	18. SECURITY CLASSIFICATION OF THIS PAGE Unclassified	19. SECURITY CLASSIFICATION OF ABSTRACT Unclassified	20. LIMITATION OF ABSTRACT	

